crystals

MDPI

Article

New EoL Routes of Al-Li Aircraft Integral LBW and FSW Welded Panels including New Cr-Free Coatings

Ana Isabel Fernández-Calvo [1,*], Clara Delgado [1], Philippe Dufour [2], Egoitz Aldanondo [3], Mario Díaz [4] and María Belén García-Blanco [4]

[1] AZTERLAN, Basque Research and Technology Alliance (BRTA), E-48200 Durango, Spain; cdelgado@azterlan.es
[2] Société Nationale de Construction Aérospatiale, SONACA SA, 6041 Gosselies, Belgium; philippe.dufour@sonaca.com
[3] LORTEK, Basque Research and Technology Alliance (BRTA), E-20240 Ordizia, Spain; egoitz@lortek.es
[4] CIDETEC, Basque Research and Technology Alliance (BRTA), E- 20014 Donostia, Spain; mdiaz@cidetec.es (M.D.); bgarcia@cidetec.es (M.B.G.-B.)
* Correspondence: afernandez@azterlan.es; Tel.: +34-946-215-470

Abstract: The end of fife (EoL) of new aircraft panels made of Al-Li alloys in which the stringers and skin were joined, either by laser beam welding (LBW) or by friction stir welding (FSW), was investigated at the lab scale. Different cutting strategies, ranging from cutting only for size reduction to full separation of all materials, including the removal of the welded seam, were defined, with the objective of recycling the maximum amount of panel scrap back into high-quality aircraft Al-Li alloys. Those welded aerostructures were coated with two novel Cr-free coating systems. The effect of the coatings on the recyclability of the panels and the need to eliminate the primer and topcoats were researched. Fading/enrichment of the alloying elements during recycling was determined. The chemical compatibility of the recycled alloys with four commercial Al-Li alloys was examined. The EoL route that maximized closed-loop recycling and the conservation of the valuable alloying elements was identified. Nine out of the ten configurations were found to be compatible with joint recycling. Only the LBW structure with ER4047 filler wire required sorting into scrap fractions and removing the weld seam. Decoating by corundum blasting followed by cutting before remelting is the recommended EoL process.

Keywords: end of life; metal recycling; aluminum–lithium alloys; light metallic alloys; aircraft fuselage; material sorting; decoating

check for updates

Citation: Fernández-Calvo, A.I.; Delgado, C.; Dufour, P.; Aldanondo, E.; Díaz, M.; García-Blanco, M.B. New EoL Routes of Al-Li Aircraft Integral LBW and FSW Welded Panels including New Cr-Free Coatings. *Crystals* **2023**, *13*, 807. https://doi.org/10.3390/cryst13050807

Academic Editor: Sanbao Lin

Received: 21 March 2023
Revised: 27 April 2023
Accepted: 6 May 2023
Published: 11 May 2023

Copyright: © 2023 by the authors. Licensee MDPI, Basel, Switzerland. This article is an open access article distributed under the terms and conditions of the Creative Commons Attribution (CC BY) license (https://creativecommons.org/licenses/by/4.0/).

1. Introduction

The third generation of Al-Li alloys with Li content between 0.75 and 1.8% [1,2] offers a wide range of opportunities for significant improvements through density reduction (~3–4% lighter) compared to conventional Al alloys, stiffness increase (~5–8%), increment in fracture toughness and fatigue crack growth resistance, and enhanced corrosion resistance. These new Al-Li alloys, in combination with advanced design concepts including the assembly by innovative laser beam welding (LBW) and friction stir welding (FSW) technologies, will make it possible to improve the structural performance of the next generation of commercial aircraft structures. These integral panels (LBW or FSW) significantly reduce the manufacturing and operational costs, structural weight, and complexity, compared to conventional riveting counterparts.

Indeed, Airbus has already implemented LBW for the manufacturing of lower fuselage panels in its A318 and A380 aircraft [3]. On the other hand, FSW has been also used in the manufacturing of fuselage structures by several aircraft manufacturers [4,5] such as EMBRAER [6]. The potential of LBW and FSW has been widely demonstrated, at least in conventional aluminum alloys such as the 6XXX and 5XXX series, showing clear benefits

over conventional joining technologies. In the case of Al-Li alloys, many works have been focused on the development of LBW and FSW for joining skin–stringer-type structures. However, many difficulties were found in obtaining defect-free welds [7,8].

Therefore, it is necessary to further develop the process to understand the mechanisms that involve the weld formation. Previous works have demonstrated the strong influence that the welding parameters and probe geometry have on the typical defect features of the friction stir welded lap joints (hook and cold lap defects) [9–11]. Moreover, it is of paramount importance to consider the effect that other manufacturing variables, such as sealant application or surface treatment, can have on the mechanical performance and manufacturability of the joints. Previous works have reported that FSW of TFSAA or sol–gel-treated third-generation Al-Cu-Li aluminum alloys combined with sealant application at the crevice of the lap joints seems to be a feasible and promising technique for the manufacturing of lightweight aeronautic structures with good corrosion resistance [12]. In addition, sealant application has been reported to improve the mechanical performance of the stringer–skin FSW joints under loop stress loading conditions compared to joints with no sealant application [13].

Targeting lower environmental impacts during the production of those novel aircraft fuselage structures, their maintenance phase, and the aircraft's end-of-life phase is crucial for developing sustainable air transport technologies. The ecodesign of the future aerostructures requires the selection of the combination of manufacturing processes and materials (Al-Li alloys, welding technologies, surface treatments) that meets the technical high-performance requirements and, simultaneously, favors recycling of the welded panels at their end of life (EoL).

Aluminum recycling has considerable environmental and economic benefits. It saves approximately 95% of the energy and associated emissions compared to producing metal from ore [14]. EoL recycling then delivers a CO2 savings of 96% [15]. In addition, one ton of recycled aluminum saves up to 8 tons of bauxite, 40 barrels (6300 L) of oil, and 7.6 m^3 of landfill space [16]. Aluminum can practically be recycled endlessly without hardly any quality loss. The recycling rate in the most important areas of use lies between 95 and 100% [17]. However, the presence of impurities and their removal pose an important challenge, restricting their final reuse to certain applications. Aluminum alloy recycling efficiency and recycling routes are heavily dependent on scrap origin and quality. Compared to many metals, aluminum presents a high degree of difficulty in the removal of tramp elements from the melt, mainly due to thermodynamic links between them which prevent their separation by the two usual recycling processes: remelting processing (for example by fading and/or oxidation) or refining under a salt (NaCl-KCl) slag by the chemical reactions with the salt product [14,18,19]. The effects of solid impurities can vary greatly according to composition and origin, which is why targeted removal is necessary prior to the solidification process. Otherwise, not only the material properties (elongation, toughness, yield strength, corrosion property, surface quality, etc.), but also the subsequent process steps, such as those during forming, can be negatively affected [19,20]. This is the reason for the importance of strategies for the removal of undesired elements from the recycled alloy by physical separation of the different materials prior to melting [19,21].

Recycling Al-Li parts makes it necessary to take other factors into consideration such as the high price of lithium, its high reactivity (high dross formation tendency and high reaction with the refractory materials), and the high fading of Li during remelting. Due to the high reactivity of lithium, the Al-Li alloys are the only ones that require a protective atmosphere during remelting and handling. If conventional, non-protective remelting is performed all Li content is lost and a high amount of sponge dross is formed. The FP7-SENTRY project [22,23] demonstrated that it is possible to obtain ingots of Al-Li alloys with possibilities to be reprocessed and transformed in the same aircraft raw materials, provided that the different aluminum alloy families present in riveted fuselage structures are separated and adequately sorted. However, the alloy separation is more complex in integral welded structures because of the presence of zones with mixed materials.

Moreover, novel Cr (VI)-free coating systems in different layers (conversion coating/anodic layer, sol–gel, primer, and topcoat) were developed in Clean Sky's ecoTECH project [24]. Thus, it was also necessary to study the effect of these new coatings in the EoL process.

There are different techniques to remove coating layers from Al structures which can be divided into mechanical (usually blasting), physical (laser treatments), and chemical (etching) methods. Laser paint stripping (LPS) has been successfully used to remove paint systems, and some solutions are already on the market [25], but the investment costs are still high and selective and customized stripping is still under development. Regarding chemical paint stripping, methylene chloride-based stripping solutions (dichloromethane, DCM) have been the most effective formulations to remove aircraft paint systems [26]. However, this process is now restricted in the EU (Annex XVII to REACH Regulation [27]). One potential alternative, which avoids the hazards of more traditional methods, is the use of benzyl alcohol-based solutions [28]. Blasting is one of the most used mechanical methods, and multitudes of abrasive materials have been used to strip paints, including sand, glass bead media, and corundum particles. Blasting with corundum and glass beads from mechanical methods and chemical stripping with benzyl alcohol-based formulation from the chemical methods have been used and compared in this work because both appear as the most common, effective, and industrially scalable removal methods.

When it comes to aircraft dismantling and recycling, the selection of a proper solution is always a trade-off between the costs of preparing the scrap for recycling and the improvement of the recycling potential. This paper presents the results of the investigation of the potential for combined recycling of several alloys joined in welded airframe structures so that sorting and separation of components can be minimized—or even avoided—and the remelted ingots obtained can be reprocessed without major composition adjustments back into Al-Li aircraft alloys. Different scrapping and decoating strategies are evaluated to define the best way to proceed in terms of environmental impact and cost. Based on the results of experimental laboratory remelting tests of scrap originating from various welded Al-Li alternatives, the theoretical closed-loop recyclability of Al-Li alloys joined by LBW and FSW was assessed. This research is part of the H2020 ReINTEGRA project, which aims at developing sustainable EoL procedures for the next generation of integral welded airframe structures made using different innovative Al-Li alloys, welding technologies, and Cr-free surface treatments and primers.

2. Materials and Methods

The welded coupons representing different combinations of Al-Li alloys and welding techniques employed in the EoL research were manufactured and supplied by Clean Sky 2 ecoTECH project. The said project had been investigating the manufacture of LBW and FSW coupons with several combinations of alloys and two different coating alternatives, as well as four stringer configurations (one for LBW coupons and three for FSW coupons, as depicted in Figure 1). In the LBW coupons, the skin and the L-shape stringer were made of the same alloy (AA2198) in all cases and five different filler wires were tested for weldability and recyclability: two commercial wires, i.e., ER4047 (AlSi11 alloy) and ER2319 (Al-Cu alloy), and three filler wires provided by the H2020-IAWAS project (GA 821371), namely ER2395 (Al-Cu-Li alloy), U817 (Al-Cu-Li alloy), and J300 (Al-Cu-Sc alloy). A double LBW joint (T-welding) was used in all references. The novel filler wire U817 did not perform satisfactorily in the coupon welding; therefore, the corresponding LBW coupon reference R4 was discarded for further study of its recyclability. For FSW coupons, two different skin alloys (AA2198 and AA2060) and three different Z-type stringer materials and dimensions were under study: AA2196 (30 mm extruded), AA2198 (30 mm forged), and AA2099 (70 mm extruded). FSW coupons were welded using Naftoseal MC-780 C sealant. For further information on the welding parameters and set-up used for developing the LBW and FSW joints, the reader is referred to a previous work [29].

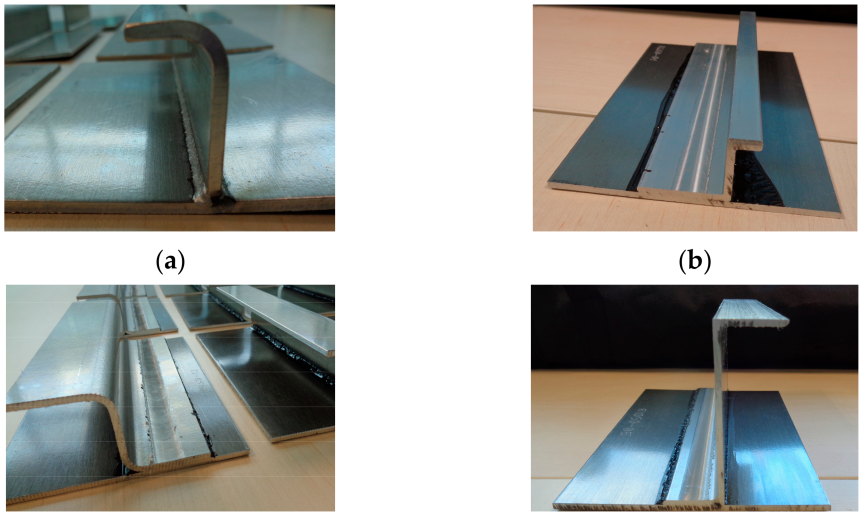


Figure 1. Photographs of the four different stringer configurations investigated (uncoated coupons): (**a**) LBW coupons R1-R5; (**b**) FSW coupons R6 and R8; (**c**) FSW coupons R7 and R9; (**d**) FSW coupons R10 and R11.

Thus, samples of four LBW coupon references and six FSW references were supplied to evaluate their closed-loop recyclability and to define the optimal EoL procedure, with the combinations of alloys, welding technologies, and stringer types described in Table 1. Uncoated specimens of the ten references were scrapped and remelted to investigate the effect of the welding joints on their recyclability into aeronautical Al-Li alloys. The LBW coupon references (R1, R2, R3, and R5) were used to determine the specific effect of each filler wire on the chemical compatibility of the LBW coupon scrap. Likewise, to examine the potential impact of the sealant applied in the FSW joints on the recyclability, FSW coupon reference R7 with skin and stringer made of the same alloy (AA2198) was tested with and without sealant. The FSW references R6, R8, R9, R10, and R11 served to evaluate chemical compatibility for recycling of pairs of Al-Li alloys in two different mass ratios (depending on the stringer dimensions). Finally, coated samples of two coupon references (LBW R1 and FSW R11) were tested to investigate the influence of the coating on the composition of remelted scrap and the need for a decoating step. Concerning the coating, two different surface treatments were applied by Hellenic Aerospace Industry in ecoTECH project [20] on coupon references R1 and R11: anodic layer (thin-film sulfuric acid anodization (TFSAA) coating) and AC-131 (sol–gel coating), plus Cr-free primer and topcoat. The number of specimens supplied for each coupon reference is listed in Table 1. In total, 161 specimens were tested for assessing potential EoL strategies. The nominal dimensions and the average weight of the coupons are indicated in Table 2.

The chemical composition of the different skins, stringers, and filler wires used in the manufacture of the 10 coupons was analyzed using inductively coupled plasma optical emission spectroscopy (ICP-OES) equipment, Thermo Scientific Icap 7400 radial model. Test conditions: power 1250, exposure time 15 s, nebulizer gas flow 0.65 L/min, and 3 samples per measurement.

The thickness of the coatings was measured by eddy current, and for this purpose, Fischer DualscopeMP20 instrument was used. Microstructure analyses were conducted using optical and SEM facilities: field emission scanning electron microscope (FESEM), ZEISS Ultra Plus microscope (CARL ZEISS AG, Oberkochen, Germany) for cross-section analysis, and SEM (JSM-5500LVmodel-Jeol s coupled with a 200 Series INCA ENERGY lead from Oxford Instruments, for the qualitative analysis of the treated surface composition). The cross-sections of all the coupons were analyzed to define the weld seam for LBW and FSW coupons.

Table 1. Summary of the 10 coupon references investigated for EoL in ReINTEGRA project.

Ref.	Skin Alloy	Stringer Alloy	Stringer Type	Welding Technology (Filler Wire)	Welding Joint	No. of Specimens
R1	AA2198	AA2198	L-30 mm (formed)	LBW (ER4047)	T	uncoated: 24 u coated S1 [b]: 8 u coated S2 [b]: 10 u
R2	AA2198	AA2198	L-30 mm (formed)	LBW (ER2319)	T	uncoated: 9 u
R3	AA2198	AA2198	L-30 mm (formed)	LBW (ER2395)	T	uncoated: 9 u
R4 [a]	AA2198	AA2198	L-30 mm (formed)	LBW (U817)	T	0
R5	AA2198	AA2198	L-30 mm (formed)	LBW (J300)	T	uncoated: 9 u
R6	AA2198	AA2196	Z-30 mm (extruded)	FSW	Overlap	uncoated: 7 u
R7	AA2198	AA2198	Z-30 mm (formed)	FSW	Overlap	uncoated: 10 u (5 u no sealant)
R8	AA2060	AA2196	Z-30 mm (extruded)	FSW	Overlap	uncoated: 16 u
R9	AA2060	AA2198	Z-30 mm (formed)	FSW	Overlap	uncoated: 16 u
R10	AA2198	AA2099	Z-70 mm (extruded)	FSW	Overlap	uncoated: 7 u
R11	AA2060	AA2099	Z-70 mm (extruded)	FSW	Overlap	uncoated: 20 u coated S1 [b]: 12 u coated S2 [b]: 4 u

[a] EoL of coupon R4 was not studied due to the quality problems of the filler wire. [b] coating S1 = TFSSA + Cr-free primer + topcoat; coating S2 = AC 131 + Cr-free primer + topcoat.

Table 2. Nominal size and average weight of coupons of the 10 references evaluated.

Ref.	Skin			Stringer					Average Mass of Specimen, g
	Length, mm	Width, mm	t_s [a], mm	Length, mm	Height, mm	Top Flange Width, mm	Bottom Flange Width, mm	t_w [b], mm	
R1 R2 R3 R5	135	100	2.5	135	30	15	-	2.5	uncoated: 128.19 R1S1 [c]: 131.06 R1S2 [c]: 130.68
R6 R8	150	100	2.5	150	25.4	10.16	31.75	2.54	uncoated: 169.47
R7 R9	150	100	2.5	150	36	33	33	2.5	uncoated: 197.59
R10 R11	150	100	2.5	150	63.5	22.23	22.23	1.98	uncoated: 188.36 R11S1 [d]: 189.38 R11S2 [d]: 188.32

[a] t_s: thickness of skin. [b] t_w: thickness of stringer web. [c] R1S1: R1 coupons coated with TFSSA, R1S2: R1 coupons coated with AC 131 sol–gel. [d] R11S1: R11 coupons coated with TFSSA, R11S2: R11 coupons coated with AC 131 sol–gel.

Four scrapping options were investigated in the present work (see Figure 2), ranging from no separation of the weld seam (0C option) to complete separation of the weld seam from the skin and stringer fractions (3C option). All cuts were performed on the premises of SONACA by abrasive cutting with a Makita 9565H hand-held angle grinder, using a Kronenflex A 60 N Supra aluminum cut-off wheel (diameter × width × bore in mm: 125 × 1 × 22.23). Specimens from every coupon reference were scrapped following the four cutting alternatives. As an example, the scrap fractions obtained by applying the

four cutting strategies 0C, 1C, 2C, and 3C on LBW R1 coupons are pictured in Figure 3. The scrap pieces forming the fractions that were directed to separate melting tests are also indicated in the figure. The excess cured sealant present on the sides of the joint of the uncoated FSW coupons supplied (discernible in Figure 1b–d) was removed before any cutting and remelting test, by first spraying acetone on the sealant and then scratching it with a plastic scraper. The coated specimens of reference R11 used in the decoating tests did not show any excess cured sealant.

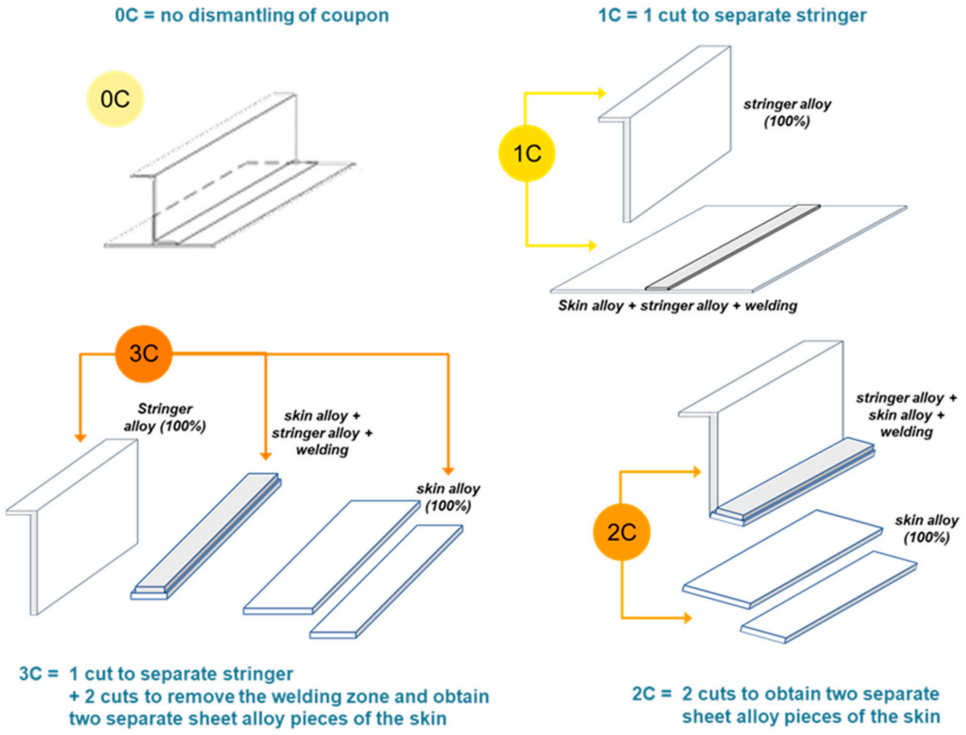


Figure 2. Schematic representations of the four cutting options applied to scrap coupons.

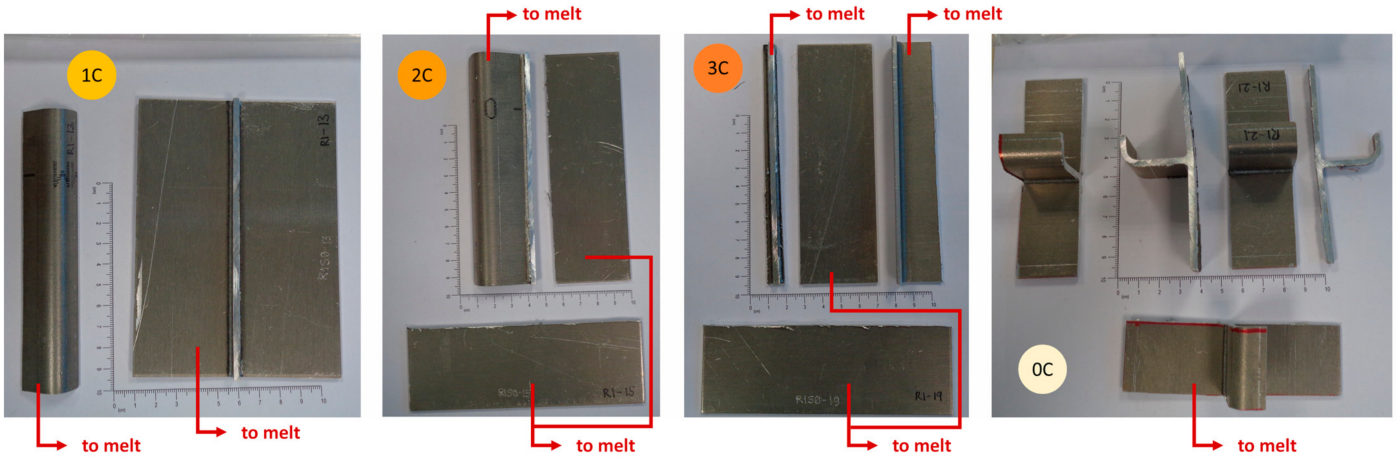


Figure 3. Example of the different scrapped fractions obtained through the four cutting strategies (0C, 1C, 2C, and 3C) for LBW R1 coupons. The sorted fractions to separate remelting tests are indicated.

For each scrap fraction sorted in the cutting experiments, an analysis sample of mass between 27 and 31 g was melted in a LIFUMAT—MET 3,3-Vac remelting unit for sample preparation for spectroscopy (LINN), under an argon protective atmosphere (5 L/min flow rate of high purity 99.999% Ar). In every remelting test, the induction furnace was kept

switched on for a few additional seconds after observing the full melting of the sample in the crucible. The total remelting time varied between 60 and 90 s depending on the weight of the sample, on the size and shape of each part inside the crucible, and on the alloys and other compounds present in the scrapped material. The molten scrap sample was cast in a metallic mold, and the chemical composition of the obtained specimen was analyzed. Most of the coupons were tested in uncoated condition, but some of them were tested in coated condition and in decoating condition after shot blasting with corundum. The metal yield was calculated as the ratio between the metal extracted in the obtained solid sample divided by the initial weight of the sample. That means not considering the dross formed during the remelting test.

To predict the compatibility of the scrap with the four base Al-Li alloys employed in manufacturing the coupons (AA2060, AA2196, AA2099, AA2198), a calculation tool based on Microsoft Excel was developed (*ReINTEGRA Scrap Recyclability Tool*) by the authors. The chemical composition of the scrap (as wt.% of each chemical element) is entered by the user. The tool, then, checks if that composition fits into the chemical composition limits of the registered alloys (TEAL Sheets, The Aluminum Association, Arlington, VA, USA, 2015) and provides an estimate of the percentage of the scrap that could be acceptable as raw material for manufacturing each of the four 3rd generation Al-Li alloys assessed (scrap recyclability, closed-loop), indicating at the same time whether any alloying elements would need additions to adjust the final composition of the alloy. It also identifies the chemical element critical for the compatibility and/or limiting the amount of scrap that can be used as raw material.

3. Results

3.1. Chemical Composition of Raw Materials

The results of ICP-OES analyses of the raw materials are displayed in Table 3. Skins and stringers are made of four different Al-Cu-Li alloys with different concentrations of Cu and Li. While the 70 mm height stringer was made of AA2099 alloy without Ag, the other three had silver as an alloying element. AA2060 and AA2198 alloys had Li content below 1 wt.%, while AA2198 and AA2099 alloys had a Li content higher than 1.60 wt.%. The Cu content varied from 2.45 up to 3.74 wt.%. The Mg content varied from 0.25 up to 0.75 wt.% and the Zn content was <0.03 in AA2198 alloy up to 0.62 wt.% in AA2099. Concerning the filler wires for LBW, one is AlSi11, two are Al-Cu and the other one is an Al-Cu-Li filler wire. Note that main impurities are very low: Si < 0.04% and Fe < 0.053 wt.%.

Table 3. Chemical composition in wt.% and density value of the different skins, stringers, and filler wires of the 10 coupons. The standard deviation values in wt.% of each measurement are provided in Table S1 of Supplementary Material.

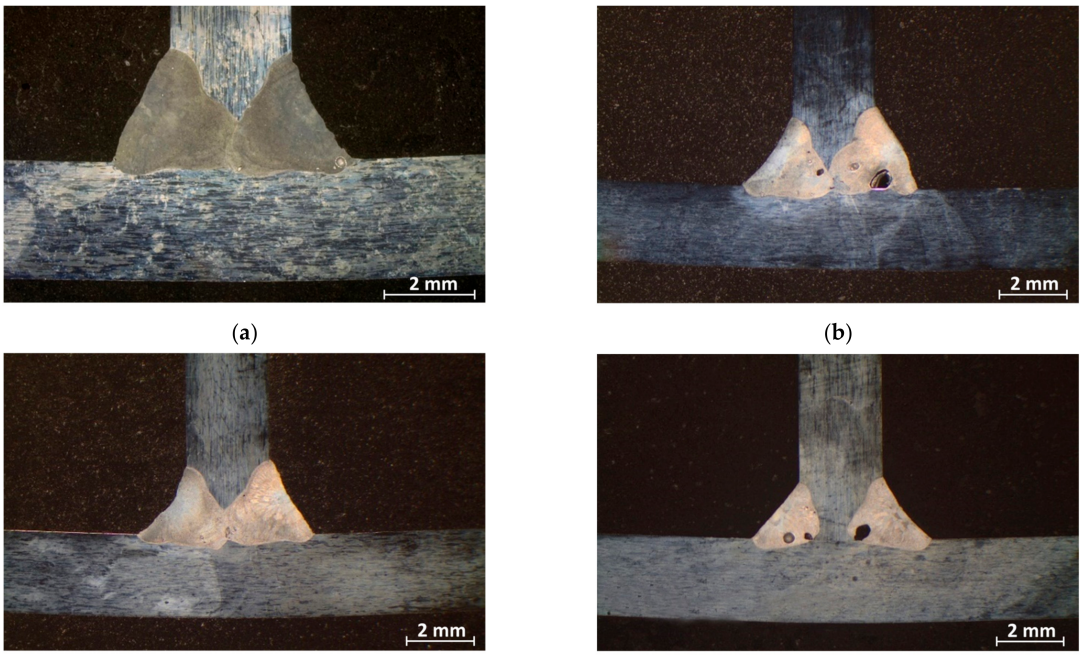
Reference	Density (g/cm^3)	Chemical Composition (wt.%)										
		Li *	Cu	Mg	Ag *	Zr *	Mn	Zn	Fe	Si	Ti *	Al
AA2060 (skin)	2.73	0.68	3.74	0.75	0.29	0.096	0.29	0.35	<0.03	<0.04	0.025	Rem.
AA2198 (skin and stringer)	2.70	0.98	3.28	0.31	0.21	0.091	<0.03	<0.03	0.041	<0.04	0.027	Rem.
AA2196 (stringer)	2.64	1.62	3.08	0.33	0.24	0.12	0.35	0.047	0.053	<0.04	0.040	Rem.
AA2099 (stringer)	2.64	1.65	2.45	0.25	<0.02	0.10	0.29	0.62	0.036	<0.04	0.030	Rem.
ER4047 (filler wire)	2.71	<0.008	<0.04	<0.03	<0.02	<0.008	<0.03	<0.03	0.18	11.4	0.013	Rem.
ER2319 (filler wire)	2.72	<0.008	5.93	<0.03	<0.02	0.11	<0.03	<0.03	0.071	0.042	0.160	Rem.
ER2395 (IAWAS) (filler wire)	2.70	1.20	3.73	0.34	0.23	0.085	<0.03	<0.03	0.046	<0.04	0.020	Rem.
J300 (IAWAS) (filler wire)	2.79	<0.03	6.32	<0.03	<0.02	0.11	0.31	<0.03	0.078	<0.04	<0.03	Rem.

* The tests marked are not covered by the ENAC accreditation.

3.2. Microstructure of Cross Weld Section of the Coupons

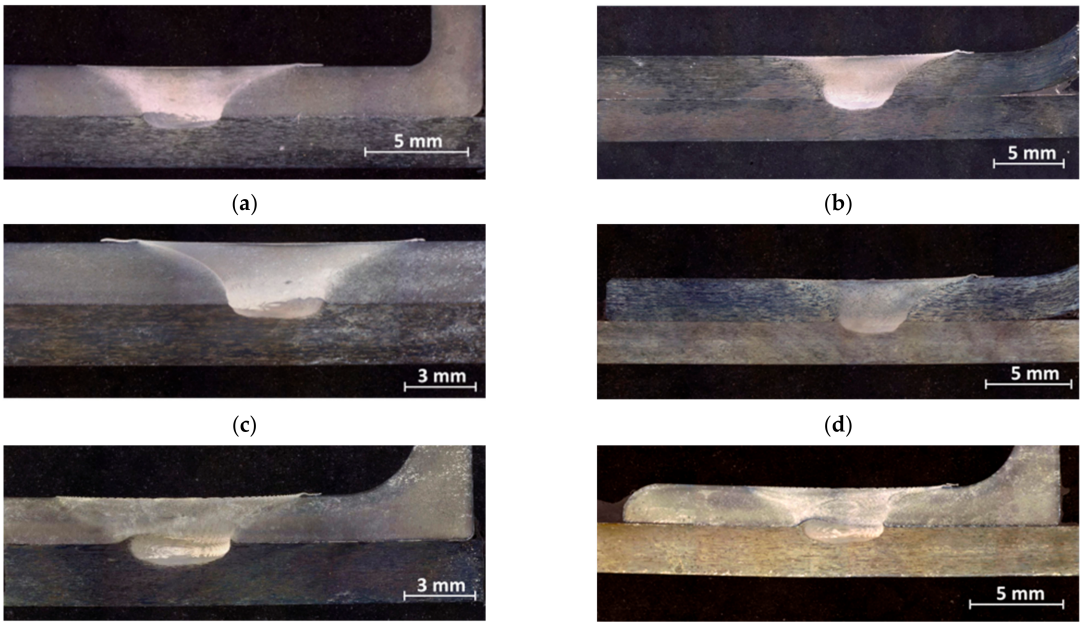
Microstructure analysis of the cross-sections was performed to define the width and height of the weld seam for LBW coupons in Figure 4 and for FSW coupons in Figure 5 after etching. This is part of the pre-scrap analysis to define the cutting margins necessary to avoid chemical contamination associated with each type of welding for the defined

EoL strategies. A detailed analysis of chemical contamination is shown for the R1 coupon cross-section in Figure 6 (SEM image) and in Figure 7a (optical image) without etching. The chemical contamination of base alloy is concentrated in a few microns next to the LBW welding seam as it is indicated in Figure 6 by the dashed line which separates the area where the microstructure of the base material is not affected for the weld seam in terms of modification of the precipitated phases. In addition, there was no contamination of the high Si present in the filler wire, and black-colored phases were not observed outside of the weld seam.



(**a**) (**b**) (**c**) (**d**)

Figure 4. Microstructures of the LBW coupons: (**a**) R1; (**b**) R2; (**c**) R3; (**d**) R5 coupons.



(**a**) (**b**) (**c**) (**d**) (**e**) (**f**)

Figure 5. Microstructures of the FSW coupons: (**a**) R6; (**b**) R7; (**c**) R8; (**d**) R9; (**e**) R10; (**f**) R11 coupons.

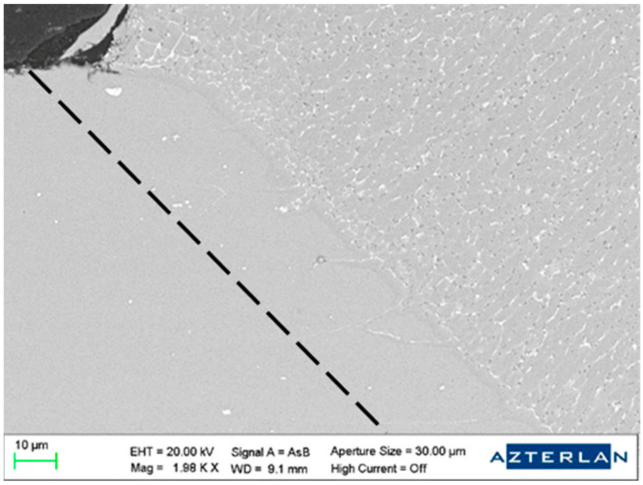


Figure 6. Cross-section of SEM micrograph of R1 coupon. The dashed line separates the base material microstructure from the region affected by the weld seam in terms of modification of precipitation phases.



(**a**) (**b**)

Figure 7. Optical micrographs: (**a**) R1 LBW and (**b**) R11 FSW coupons without etching. Red lines indicate the cutting margins necessary to avoid chemical contamination and geometry limitations. Note: The external marks associated with the FSW process are framed in a white rectangle. The green rectangle indicates the full mixed area.

The optical micrograph of the R11 coupon is shown in Figure 7b (optical image). The external marks associated with the FSW process are framed in a white rectangle and have a width of around 11 mm. The green rectangle indicates the full mixing zone of the two aluminum materials with a width of about 5 mm. In addition, traces of the FSW weld sealant (black-colored) are observed along the entire cross-section. The red lines of Figure 7 indicate the cutting margins to avoid chemical contamination and geometrical limitations for LBW and FSW configurations.

3.3. Coating Effect on EoL of Integral Weld Panels

Table 4 presents the thickness of the different layers of the coating systems with TFSSA and sol–gel, obtained by SEM image analysis and eddy current method.

Table 4. Coating thickness measured using SEM and eddy current.

Coating System	Face	Thickness SEM Analysis				Eddy Current Thickness (µm)
		1st Coating (µm)	Primer (µm)	Topcoat (µm)	Total (µm)	
TFSAA	A	3.2 ± 0.2	8.6 ± 1.4	8.0 ± 1.5	19.7 ± 2.0	17.1 ± 1.3
	B	3.5 ± 0.3	7.2 ± 1.6	19.2 ± 2.3	29.9 ± 2.8	25.5 ± 1.5
AC131 (sol–gel)	A	<0.5	5.2 ± 0.8	14.4 ± 0.9	19.6 ± 1.3	17.5 ± 2.6
	B	<0.5	6.6 ± 1.7	11.3 ± 1.7	17.9 ± 2.4	15.1 ± 2.3

The cross-section micrographs obtained using an SEM for both coating systems are detailed in Figure 8.

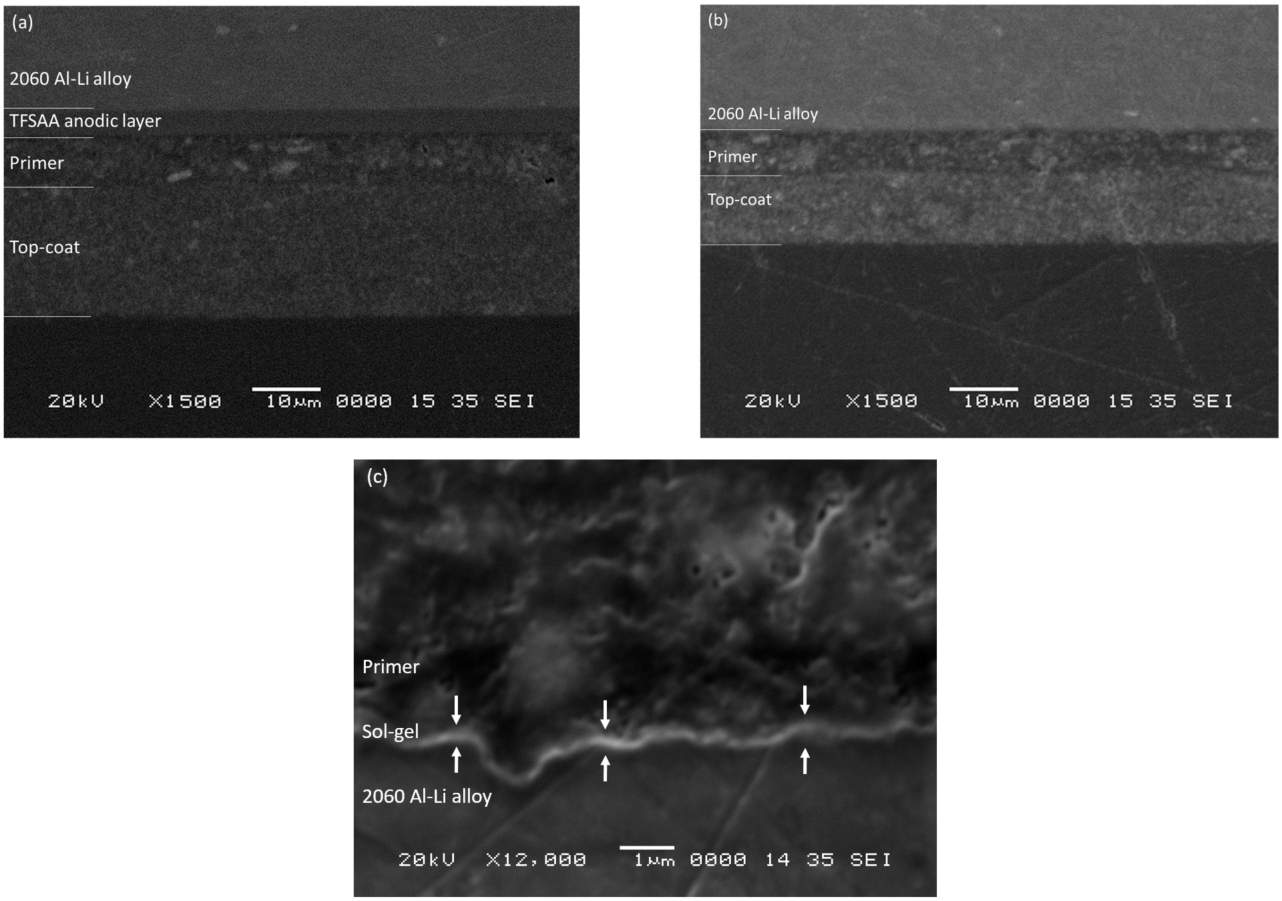


Figure 8. SEM images of AA2060-T8E30 with different coating structures: (**a**) TFSAA + primer + topcoat, (**b**) AC131 + primer + topcoat, and (**c**) detail of the AC131 sol–gel layer marked with arrows between Al-Li alloy substrate and primer.

The chemical composition of each coating was investigated by EDX analysis (see Figure 9). The TFSAA layer is rich in S and Al. The sol–gel layer is rich in Si and Zr. The primer is rich in Ti particles and C. The topcoat is rich in Mg and Ti-particles and Fe. A small amount of C is also observed in the primer and topcoat.

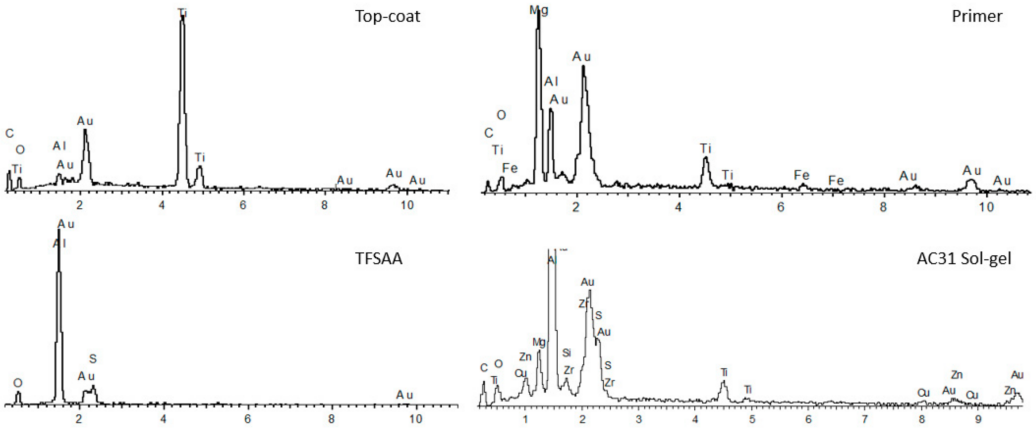


Figure 9. EDX spectra of the different coatings.

The summary of the decoating tests performed for both coating systems carried out by corundum blasting, glass beads blasting, and chemical stripping processes using a benzyl-alcohol-based formulation is shown in Table 5. Chemical stripping was able to remove the coating system with TFSAA properly, but the complete removal of the sol–gel coating could not be achieved. All the coatings were completely removed by the blasting process; however, the use of corundum blasting showed better performance in terms of processing rate and cost, as shown in Table 5.

Table 5. Results of chemical stripping and blasting experiments on decoating of both TFSAA and sol/gel coatings.

Process	Conditions	TFSAA	AC131
Blasting	• Corundum (106–150 µm) • 7 bar, 1.5 dm^2 min^{-1}	Full stripping ΔW * (%) = 1.44%	Full stripping ΔW (%) = 1.18%
	• Glass beads (40–70 µm) • 7 bar, 1.5 dm^2 min^{-1}	Full stripping ΔW * (%) = 1.08%	Full stripping ΔW (%) = 1.05%
Chemical Stripping	• Stripping: 80 °C, 60 min, air agitation • Desmutting: HNO_3 (30%), 25 °C, 2 min	Full paint removal, remains of anodic layer ΔW * (%)~1.2%	Non-scalable Very long processing times
	• Stripping: 80 °C, 60 min, air agitation • Desmutting: HNO_3 (30%), 25 °C, 2 min • Deanodizing: NaOH (50 gL^{-1}) 40 °C, 2 min • Desmutting: HNO_3 (30%) 25 °C, 2 min	Full stripping ΔW * (%)~1.5%	

* ΔW (%) is the percentage of weight reduction due to the decoating process.

A comparison between the processing rate and abrasive consumption of blasting with corundum and glass beads has been performed in order to evaluate the performance of both processes (Table 6).

Table 6. Processing rate and abrasive consumption for full coating stripping with blasting at 7 bar.

Blasting Abrasive Media	Corundum	Glass Beads
Average processing rate Total stripped area/total blasting time (dm^2/min)	1.63	0.54
Abrasive consumption Abrasive waste produced per m^2 of treated surface (kg/m^2)	~2.6	~10

Coated and decoated coupons after corundum blasting are shown in Figure 10. The results of the remelting tests of coated samples, decoated samples with corundum, and uncoated samples for both Cr-free coatings (TFSAA and sol–gel) are shown in Table 7. A high amount of dark fumes and a high amount of slag are observed in the coated samples in comparison with the uncoated and decoated samples. The metal yield of both coated samples (TFSAA and sol–gel) was lower than the metal yield measured in the decoated samples and lower than the metal yield of the uncoated coupon (see Table 7). Silicon contamination in R1 coupons coated with TFSAA is not associated with the coating, it is associated with the filler wire that has 11 wt.% of Si. Carbon content is a little bit higher in both coated samples after remelting. No other contamination or increased loss of the usual alloying elements or impurities is observed in both coatings even in Ti, Mg, and S. The S content is the same, below 0.005 wt.% in all cases.

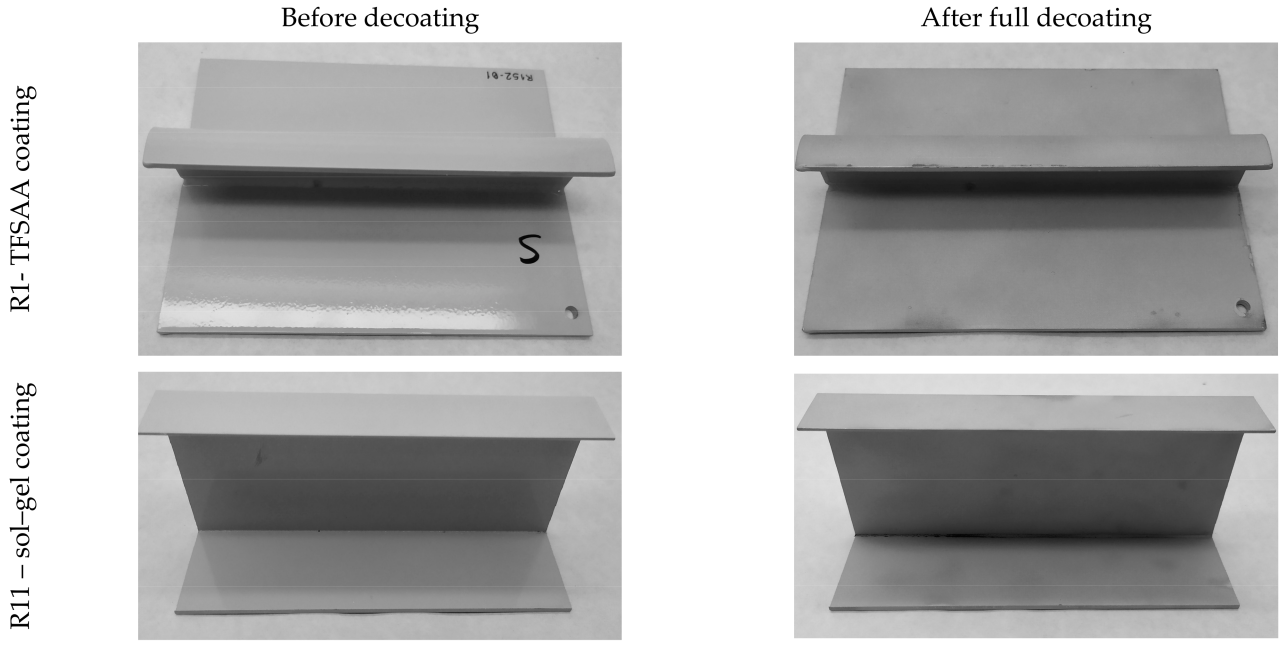


Figure 10. Coated and decoated coupons after corundum blasting.

Table 7. Comparison of chemical composition in wt.% and metal yield of remelted samples: coated samples (TFSAA and sol–gel), decoated samples, and uncoated samples. The standard deviation values in wt.% of each measurement are provided in Table S2 of Supplementary Material.

Reference	MetalYield (%)	Chemical Composition (wt.%)												
		Li *	Cu	Mg	Ag *	Zr *	Mn	Zn	Fe	Si	Ti *	C	S	Al
Uncoated (R1)	93.5	0.69	3.32	0.20	0.23	0.13	<0.03	<0.03	0.041	0.07	0.03	0.013	<0.005	Rem.
TFSAA coat (R1)	86.4	0.64	3.48	0.21	0.27	0.1	<0.03	<0.03	0.035	0.05	0.035	0.023	<0.005	Rem.
TFSAA decoat (R1)	91.1	0.73	3.54	0.22	0.29	0.12	<0.03	<0.03	0.041	0.05	0.031	0.011	<0.005	Rem.
Uncoated (R11)	94.1	1.00	3.03	0.41	0.13	0.10	0.28	0.42	0.031	<0.04	<0.03	<0.010	<0.005	Rem.
Sol–gel coat (R11)	90.0	0.78	3.15	0.36	0.19	0.11	0.29	0.47	<0.03	<0.05	0.03	0.023	<0.005	Rem.
Sol–gel decoat (R11)	91.7	0.73	3.23	0.38	0.19	0.12	0.29	0.44	0.03	0.06	<0.03	0.019	<0.005	Rem.

* The tests marked are not covered by the ENAC accreditation.

3.4. Analysis of the Different EoL Strategies

In order to select, for each coupon reference, the scrapping strategy that maximizes the amount of scrap chemically compatible with aeronautical Al-Li alloys, while minimizing cutting needs, the recyclability of the fraction scraps generated by applying the four cutting strategies was evaluated in the order 0C < 1C < 2C < 3C. When the scrap obtained in the 0C strategy for a coupon reference was found to be incompatible with Al-li alloys, the EoL strategies achieving further separation of the different alloys in the structure were investigated.

Four EoL strategies, namely 0C, 1C, 2C, and 3C, were evaluated by remelting tests of each scrap fraction for R1 coupons. The results of the remelting tests are shown in Table 8:

- 3C: weld seam fraction (fr.) (T-joint ER4047) + stringer AA2198 stump + skin AA2198 stumps;
- 2C: stringer AA2198 including weld seam (T-joint ER4047) + skin AA2198 stumps (cutting margins);
- 1C: skin AA2198 including weld seam (T-joint ER4047) + stringer AA2198 stump (cutting margin);
- 0C: coupon slice.

Table 8. Chemical composition in wt.% and metal yield of remelted samples: 0C scrapping strategy for all coupons and 1C, 2C, and 3C scrapping strategies for R1 coupon. The standard deviation values in wt.% of each measurement are provided in Table S3 of Supplementary Material.

Reference	Metal Yield (%)	Chemical Composition (wt.%)										
		Li *1	Cu	Mg	Ag *1	Zr *1	Mn	Zn	Fe	Si	Ti *1	Al
R1 3C—skin (AA2198) *2	92.3	0.61	3.22	0.2	0.22	0.11	<0.03	<0.03	0.046	<0.04	0.030	Rem.
R1 3C—stringer (AA2198) *2	93.4	0.79	3.20	0.24	0.22	0.10	<0.03	<0.03	0.040	<0.04	0.031	Rem.
R1 3C: weld fr. *2	93.6	0.57	2.99	0.18	0.21	0.10	<0.03	<0.03	0.047	0.66	0.030	Rem.
R1 2C: stringer + weld	94.4	0.66	3.26	0.20	0.22	0.10	<0.03	<0.03	0.042	0.17	0.030	Rem.
R1 1C: skin + weld	95.3	0.78	3.22	0.23	0.23	0.11	<0.03	<0.03	0.040	0.11	0.031	Rem.
R1 0C	93.3	0.78	3.23	0.23	0.23	0.11	<0.03	<0.03	0.040	0.12	0.031	Rem.
R2 0C	93.0	0.70	3.21	0.21	0.22	0.10	<0.03	<0.03	0.056	<0.04	0.031	Rem.
R3 0C	94.9	0.76	3.15	0.22	0.22	0.10	<0.03	<0.03	0.044	<0.04	0.030	Rem.
R5 0C	93.1	0.58	3.21	0.17	0.22	0.11	<0.03	<0.03	0.038	<0.04	0.030	Rem.
R6 0C	93.7	0.72	3.08	0.20	0.23	0.12	0.12	<0.03	0.042	0.048	0.035	Rem.
R7 0C	95.5	0.84	3.23	0.24	0.24	0.11	<0.03	<0.03	0.034	<0.04	0.031	Rem.
R8 0C	93.9	0.79	3.33	0.44	0.27	0.10	0.28	0.21	0.034	<0.04	0.034	Rem.
R9 0C	92.9	0.38	3.48	0.28	0.26	0.11	0.15	0.15	0.031	<0.04	0.030	Rem.
R10 0C	92.6	0.98	2.81	0.20	0.12	0.10	0.13	0.27	0.059	<0.04	0.030	Rem.
R11 0C	92.6	0.68	3.09	0.34	0.16	0.12	0.28	0.42	0.039	<0.04	<0.03	Rem.

*1 The tests marked are not covered by the ENAC accreditation. *2 These samples were analyzed in decoated state: sol–gel coating eliminated by corundum blasting. The other samples were analyzed in uncoated state.

Table 8 also shows the chemical composition in wt.% and metal yield of remelted samples for the 0C scrapping strategy for all coupons in the uncoated state. The admissible range of alloying elements, maximum values for alloying, and impurity level of the four Al-Cu-Li raw material alloys according to Teal sheets were analysed [30]. Note that AA2198 alloy is named a scrap-tolerant alloy because it has high impurity content in Si (0.12 wt.%) and Fe (0.10 wt.%).

Si content in all the scrap fractions of R1 that contain the weld seam is above 0.11 wt.%; thus, it is above the Si threshold for AA2198 alloy (raw material of its skin and stringer). Si is below 0.05 wt.% for the AA2198 skin and stringer fraction and for the other nine coupons in the 0C cutting strategy.

4. Discussion

The total thicknesses of the coating systems shown in Table 4 measured by both techniques (SEM image analysis and eddy current method) are similar, so the use of the eddy current method, as a non-destructive technique, to characterize the thickness of the tested "TFSAA + primer + topcoat" and "sol–gel + primer + topcoat" coatings was validated.

As it was shown in Tables 5 and 6, corundum blasting, in comparison with chemical stripping and glass bead blasting, showed better performance in terms of the capability of removal of all types of coatings at a higher processing rate and consuming a lower quantity of abrasive media. In this context, corundum blasting was selected as the decoating process for remelting tests in the present work.

Concerning the effect of coatings on recyclability, and based on the lower metal yield observed in coated samples after remelting tests (see Table 8), it is concluded that decoating was necessary before performing remelting/recycling tests. No other contamination or increased loss of the usual alloying elements or impurities was observed in the remelting tests shown in Table 8 in the decoated state after corundum blasting for both coatings. Thus, blasting with corundum was defined by Cidetec as the best decoating process for both Cr-free coatings, before remelting tests.

The high Si content (11.4%) in the ER4047 filler wire makes it chemically incompatible with Al-Li alloys from a closed-loop recycling point of view. As the results of the chemical

analyses of the hybrid fractions containing the weld joint have shown (Table 8), the Si content is always above the accepted upper limits for Al-Cu-Li alloys. Hence, full separation of the weld seam (3C EoL strategy) is necessary for R1 LBW coupons with Al11Si filler wire, to avoid downcycling the whole coupon into low-grade AlSiCu casting alloys typically used in high-pressure die casting (HPDC). In this way, by applying the 3C strategy, only the weld seam fraction (made up of the joint and the attached stumps of skin and stringer left after cutting) would be directed to downcycling, while a pure AA2198 scrap fraction formed by the separated skin and stringer scrap pieces could be recycled back into aeronautical Al-Li alloys. That scrap fraction (designated as R1 3C-AA2198 fr in Table 9) amounts to ca. 90% by weight of the total mass of scrap coming from R1 coupons (63.46% from the two skin pieces and 25.29% from the stringer piece). In addition, there are various detrimental aspects of recycling Al-Li alloys into lower-end HPDC alloys. One is the loss of valuable alloying elements such as lithium and silver (the measured content of Li in the weld seam fraction of R1 coupons was 0.57 wt.%, and the Ag content was 0.21%). Another is caused by the 0.57% Li content in the scrap: since the industrial recycling practice is not performed in a protective atmosphere, the Li will be oxidized and a high amount of sponge dross will be formed.

Table 9. Results of the theoretical closed-loop recyclability assessment of remelted sorted scrap fractions obtained from each coupon reference under its recommended cutting strategy (Excel-based ReINTEGRA Scrap Recyclability Tool) and the metal yields in their melting trials.

wt.% Total Coupon Scrap	Coupon Scrap Fraction	Metal Yield, %	Max.% Scrap into Charge for Target Aeronautical Al-Li Alloys (TEAL Sheets)			
			AA2198	**AA2196**	**AA2060**	**AA2099**
88.74%	R1 3C-AA2198 fr	92.61%	**100%**	100%	100%	
63.46%	*R1S2d 3C skin*	*92.30%*	***100%***	*100%*	*100%*	
25.29%	*R1S2d 3C stringer*	*92.40%*	***100%***	*100%*	*100%*	
11.26%	R1S2d 3C-weld fr	93.60%	0%	0%	0%	0%
100%	R2 0C	93.00%	**100%**	100%	100%	
100%	R3 0C	94.90%	**100%**	100%	100%	
100%	R5 0C	93.10%	**100%**	100%	100%	
100%	R6 0C	93.70%	**100%**	**100%**	100%	
100%	R8 0C	93.90%	100%	**99.10%**	**100%**	
100%	R9 0C	92.90%	**100%**	94.83%	**100%**	
100%	R10 0C	92.60%	**100%**	100%	91.84%	
100%	R11 0C	92.60%	83.33%	83.33%	**100%**	

Bold numbers indicate closed-loop recycling into one of the base alloys of the coupon.

With regard to the potential effect of the FSW sealant on the recyclability of Al-Li alloys, it is interesting to note that there is not a higher impurity content in the R7 coupon, which is an FSW coupon entirely made of AA2198 alloy, with a sealant favoring solid state welding, when it is compared with the remelting tests results of AA2198 alloy from the skin and from the stringer.

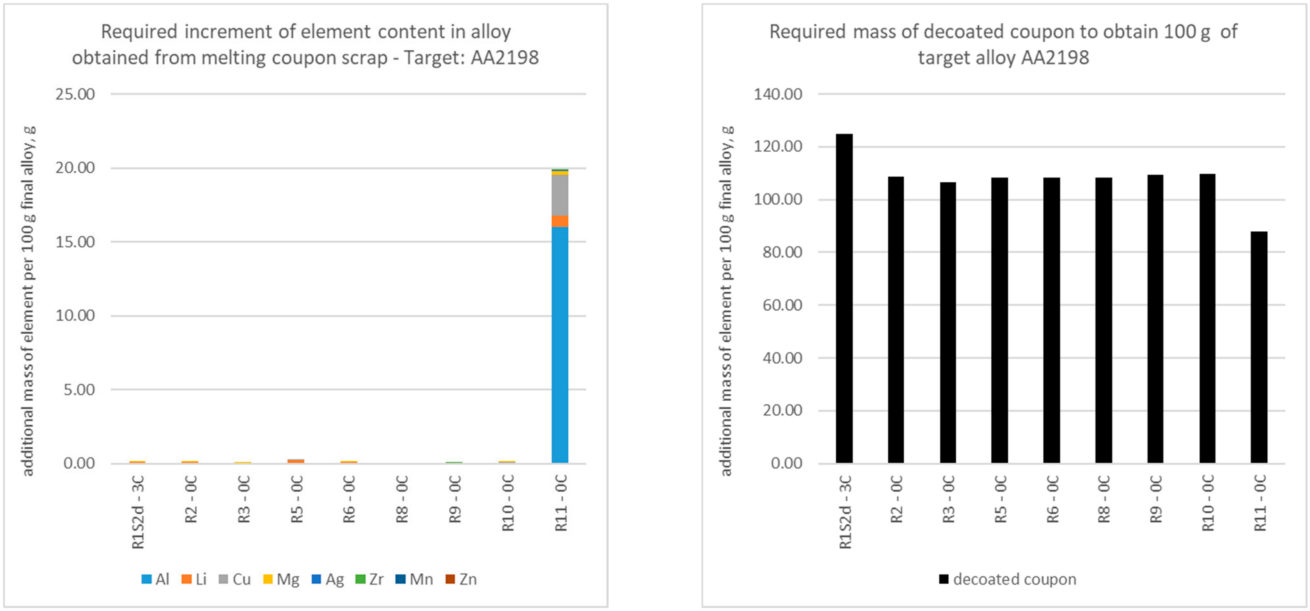
The predicted recyclability into the four base Al-Li alloys of the scrap fractions coming from the correspondingly recommended 0C and 3C cutting strategies from the various coupons is listed in Table 10. Based on the output of the Scrap Recyclability Tool, the chemical adjustment results for closed-loop recycling into AA2198, AA2196, and AA2060 are graphically represented in Figures 11–13, respectively. Table 10 presents the predicted composition corrections of the selected scrap fractions to be recycled into AA2198 alloy represented in Figure 11.

Table 10. Example of element additions (g per 100 g of molten scrap in charge) for recycling scrap fractions into AA2198 alloy (wt.%). The metal yield obtained in the remelting test is also listed because it is necessary for the calculations of the additions.

wt.% Total Coupon Scrap	Coupon Scrap Fraction	Metal Yield, %	Chemical Element Additions to Molten Scrap in Charge (wt.%)							
			Al	Li	Cu	Mg	Ag	Zr	Mn	Zn
88.74%	R1 3C-AA2198 fr	92.61%		0.10%		0.03%				
63.46%	*R1S2d 3C skin*	*92.30%*		*0.19%*		*0.05%*				
25.29%	*R1S2d 3C stringer*	*92.40%*		*0.01%*		*0.01%*				
11.26%	R1S2d 3C-weld fr	93.60%								
100%	R2 0C	93.00%		0.10%		0.04%				
100%	R3 0C	94.90%		0.04%		0.03%				
100%	R5 0C	93.10%		0.22%	0.08%					
100%	R6 0C	93.70%		0.08%		0.05%				
100%	R8 0C	93.90%		0.01%						
100%	R9 0C	92.90%		0.07%				0.03%		
100%	R10 0C	92.60%			0.09%	0.05%				
100%	R11 0C	92.60%	20%	0.12%						−0.07%
melt mass basis for recalculated additions: 120 g	*additions need to molten charge, % recalculated after dilution*			*0.79%*	*2.87%*	*0.25%*	*0.10%*	*0.04%*	*0.00%*	*0.00%*

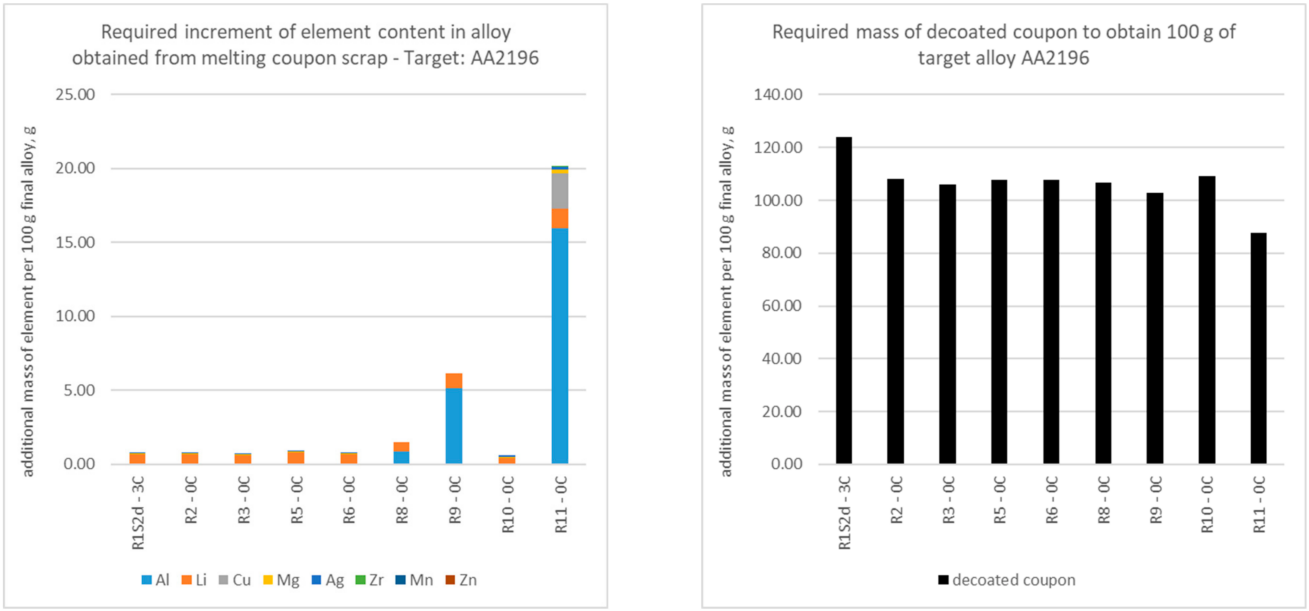
The main results for all EoL fractions shown in Table 9 (apart from the weld fraction of R1 at 3C) are summarized as follows:

- Closed-loop recycling alloy: recycling the coupons back into their base alloys (see bold numbers in Table 9) was possible, except for R10 and R11 which had an AA2099 stringer (Ag contents in the scrap from alloys AA2198, AA2196, and AA2060 are impurities for AA2099 alloy without Ag).
- The three alloys AA2198, AA2196, and AA2060 could be manufactured with the recycled material. The addition of different alloying elements will be necessary to counteract the loss of high fading elements, such as Li and Mg, and for achieving the required range of alloying elements. The alloying additions are listed in Table 10 and Figure 11 for AA2198 alloy, in Figure 12 for AA2196 alloy, and in Figure 13 for AA2060 alloy. These figures also show the required mass of the decoated coupon to obtain 100 g of target alloy.
- Dilution with pure aluminum was only necessary to manufacture AA2198 alloy for R11 scrap fraction, to manufacture AA2196 alloy for R9 and R11 scrap fractions, and to manufacture AA2060 alloy for R10 scrap fraction. When an excess of an alloying element makes it necessary to dilute the scrap with aluminum in the charge for the furnace, the correction of the contents of the other alloying elements after dilution is estimated in a second calculation run. The bottom row illustrates the first correction (pre-dilution) run and the results of the second correction (post-dilution) run for coupon R11.
- AA2198 pieces of R1 coupon could be closed-loop recycled to the base alloy, but they could also be recycled into AA2196 or AA2060. However, environmental impacts are higher because this requires the addition of some alloying elements (compare Figures 11–13).



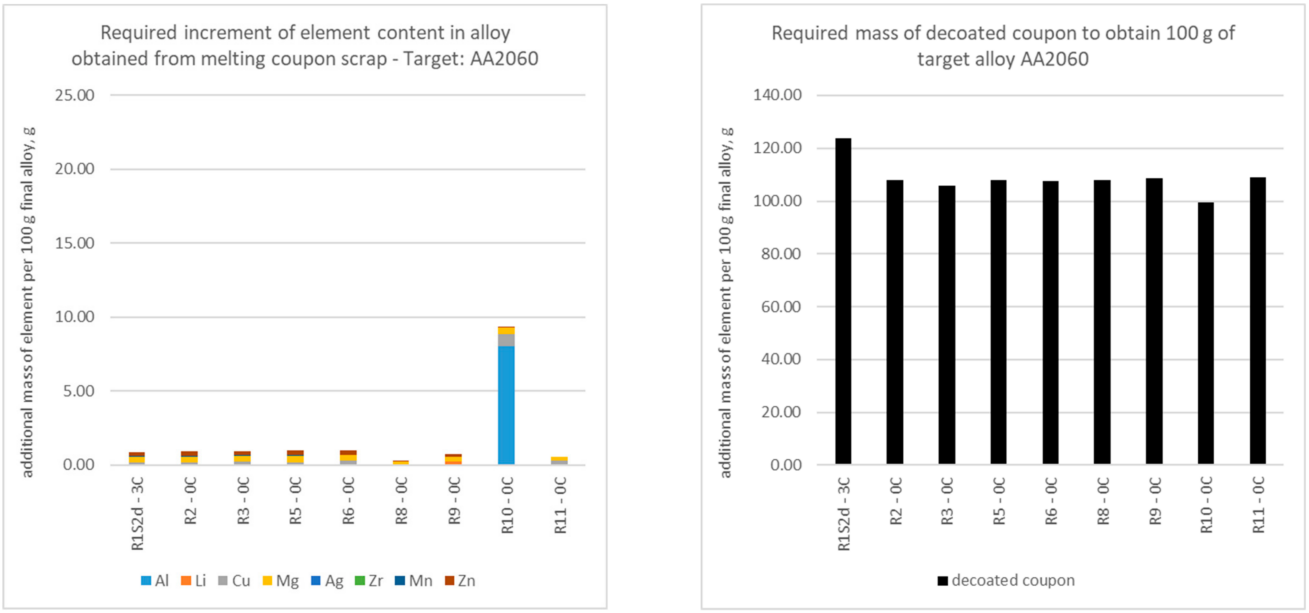
(**a**) (**b**)

Figure 11. Adjustments for closed-loop recycling scrap fractions into AA2198 per coupon reference: (**a**) required addition of alloying elements; (**b**) required mass of decoated coupon scrap to produce 100 g of adjusted AA2198 alloy.



(**a**) (**b**)

Figure 12. Adjustments for closed-loop recycling scrap fractions into AA2196 per coupon reference: (**a**) required addition of alloying elements; (**b**) required mass of decoated coupon scrap to produce 100 g of adjusted AA2196 alloy.



(**a**) (**b**)

Figure 13. Adjustments for closed-loop recycling scrap fractions into AA2060 per coupon reference: (**a**) required addition of alloying elements; (**b**) required mass of decoated coupon scrap to produce 100 g of adjusted AA2060 alloy.

4.1. Recycling into AA2198 Alloy

R11 coupon scrap from the 0C strategy is the most incompatible one to be recycled into AA2198 alloy (see Table 10 and Figure 11). Dilution with pure aluminum was necessary for the R11 coupon to diminish the excess of Zn. Thus, around 20 wt.% of pure aluminum was added plus the other alloying elements required for recycling into AA2198 alloy. Note that Zn addition was not necessary for the selected dilution rate. Concerning the required mass of the decoated coupon to obtain 100 g of target alloy AA2198 is higher than 120 g for the R1 coupon because the weld fraction is removed from the closed-loop recycling. For R2-R10 coupons, slightly above 100 g is the required mass just to recover the metal loss observed in the remelting tests. For the R11 coupon, above 88 g is the required mass because dilution was necessary to reduce the excess Zn content.

4.2. Recycling into AA2196 Alloy

AA2196 alloy is named a scrap-tolerant alloy because it has the highest impurity limits (0.12 wt.% for Si and 0.15 wt.% for Fe), as is shown in Figure 12. All the scrap required at least the addition of Li. R8, R9, and R11 0C scrap requires dilution because of the higher Cu content for R8 and R9 and because of Zn for R11. Figure 12 showed that, for comparison, R11 is the most incompatible one from the recycling point of view because it required the highest addition in weight percent and other alloying elements to obtain 100 g of the required target alloy.

4.3. Recycling into AA2060 Alloy

Manufacturing AA2060 alloy from coupon scrap required the addition of a small amount of Zn and Mg in all cases, plus the addition of Li and/or Cu or Mn, as shown in Figure 13. For comparison, R10 is the most incompatible one from a closed-loop recycling point of view because it required the highest addition in weight percent of aluminum and other alloying elements to obtain 100 g of the required target alloy.

4.4. Recycling into AA2099 Alloy

Producing AA2099 alloy from the selected hybrid coupon scrap is discarded. That alloy only allows for 0.05 wt.% Ag as a maximum in its composition, and as all the coupons contain at least one Ag-containing scrap in the charge, the scrap will contain Ag and would require high levels of dilution and, then, alloying adjustment, all of which would make that recycling option less resource- and cost-efficient than others.

4.5. Effect of Filler Wire in LBW Coupons

All filler wires except for ER4047 (high %Si, 11.4 wt.%) were compatible with AA2198 Al-Li alloy, used for skin and stringer, for closed-loop recycling. The R1 LBW coupon with ER4047 filler wire required weld seam separation from skin and stringer fractions. That means that in the 3C EoL option, skin and stringer fractions free of weld seam could be closed-loop recycled to Al-Cu-Li alloys, while the weld seam fraction will be downcycled to low-grade cast alloys.

On the other hand, R2, R3, and R5 LBW coupons with ER2319 (Al-Cu alloy), ER2395 (Al-Cu-Li alloy), and J300 (Al-Cu alloy) did not need cutting for sorting into material fractions. Apart from closed-loop recycling into the base alloy AA2198, they could be also recycled to manufacture AA2196 or AA2060 alloy. Concerning furnace charge, no dilution is needed for all cases. The same results were applicable to skin and stringer fractions of the R1 coupon.

4.6. Recyclability of FSW Weld Coupons of Two Different Al-Cu-Li Alloys

The R6, R8, R9, R10, and R11 FSW coupons did not require a scrapping–sorting strategy. That means that weld overlap separation is not needed and the 0C EoL strategy was valid for all of them. For closed-loop recycling of alloys, recycling the coupons back into their base alloys is possible, except for the AA2099 alloy (Ag contents in the scrap from AA2198, AA2196, and AA2060 alloys are impurities for AA2099 alloy). Note that Ag is a valuable element that is important to recover.

In addition, for every FSW coupon reference, there are some Al-Cu-Li recycling options that do not require dilution. Thus, a 95% energy saving vs. aluminum primary production was expected, along with savings from recovering other alloying elements such as Li, Ag, Zr, and Cu.

4.7. Definition of the Best EoL for LBW and FSW Demo Panels

The defined EoL route for FSW and LBW demo panels is summarized in Figure 14, consisting of decoating, followed by size reduction (by cutting), followed by remelting to close the loop of recycling to Al-Li aircraft alloy. The 3C cutting strategy is the best one for the LBW R1 coupon with a full separation of the weld seam. However, the other nine investigated coupons are closed-loop recyclable into Al-Cu-Li alloys without any welding separation.

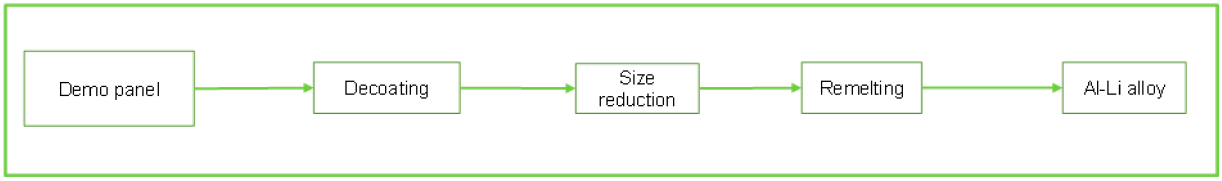


Figure 14. Defined EoL route for FSW and LBW demo panels investigated in the present work.

5. Conclusions

The main conclusions reached in the present work for the EoL of different LBW and FSW coupons, some of them coated with Cr-free coatings to obtain the highest recovery ratio of the most valuable metals, such as Li and Ag, and achieving high-grade valuable

recycled aluminum alloys from metal scrap are summarized below. Four LBW coupons, six FSW coupons, and two Cr-free coatings were tested.

- The best EoL procedures for each type of LBW or FSW welded panel were defined, consisting of decoating, followed by size reduction (by cutting), followed by remelting to close the loop of recycling to Al-Li aircraft alloy.
- The R2, R3, R5, R6, R8, R9, R10, and R11 coupons (three of them LBW coupons and five of them FSW coupons) did not require a scrapping–sorting strategy. That means that weld overlap separation is not needed and the 0C EoL strategy was valid for all of them.
- The R1 LBW coupon with ER4047 filler wire (high %Si, 11.4 wt.%) required weld seam separation from skin and stringer fractions. That means the 3C EoL option. Skin and stringer fractions free of weld seam could be closed-loop recycled to Al-Cu-Li alloys while weld seam fractions will be downcycled to low-grade cast alloys.
- The procedures defined for recycling integral welded panels welded either by FSW or LBW avoid downcycling with the exception of 11% of the LBW coupon welded with a high Si content filler wire (ER4047). With the exception of this 11%, all the Li and Ag content present in the mixed scrap was fully valorized to manufacture high-quality Al-Cu-Li aircraft alloys.
- Cr-free coating effects in closed-loop recyclability of aeronautical Al-Li alloys were as follows:
- Decoating before remelting was necessary to improve metal yield.
- Corundum blasting is an effective decoating method for both TFSAA and sol–gel coatings + primer + topcoat.
- Target Al-Li alloy in closed-loop recycling:
- Either AA2198, AA2196, or AA2060 can be manufactured using coupon scrap as a charge for the furnace. Coupon R11 scrap is the least recommended for recycling into AA2198 and AA2196; coupon R10 scrap is the least recommended for recycling into AA2060 because dilution is required.
- Producing AA2099 alloy from hybrid coupon scrap is discarded because all the scrap fractions contain Ag and this alloy only allows for 0.05 wt.% Ag as a maximum in its composition.

Supplementary Materials: The following supporting information can be downloaded at: https://www.mdpi.com/article/10.3390/cryst13050807/s1. Standard deviation values in wt.% of each measurement of chemical composition are shown in Table S1; Tables S2 and S3 are for data shown in Tables 3, 7 and 8. ± symbol refers to the expanded uncertainties calculated for a 95% confidence interval (k = 2).

Author Contributions: Investigation, P.D., C.D., E.A., M.D. and M.B.G.-B.; writing—original draft preparation, A.I.F.-C.; writing—review and editing, C.D. All authors have read and agreed to the published version of the manuscript.

Funding: This research was funded by the Clean Sky 2 Joint Undertaking (JU) under grant agreement No 886609 (ReINTEGRA project). The JU receives support from the European Union's Horizon 2020 research and innovation programme and the Clean Sky 2 JU members other than the Union.

Acknowledgments: All LBW and FSW coupons were provided by the project ecoTECH project within the AIRFRAME ITD of the Clean Sky 2 programme of H2020. Two of the filler wires, namely ER2395 (Al-Cu-Li alloy) and J300 (Al-Cu alloy), were provided by the Clean Sky 2 Joint Undertaking (JU) under grant agreement No. 821371 (IAWAS project).

Conflicts of Interest: The authors declare no conflict of interest. The funders had no role in the design of the study; in the collection, analyses, or interpretation of data; in the writing of the manuscript; or in the decision to publish the results.

References

1. Eswara Prasad, N.; Gokhale Amol, A.; Wanhill, R.J.H. *Book Aluminium-Lithium Alloys*; Processing, Properties and Applications; Merken, S., Freeland, J., Eds.; Elsevier: Oxford, MS, USA, 2014.
2. Rioja, R.J.; Liu, J. The evolution of Al-Li base products for aerospace and space applications. *Metall. Mater. Trans. A* **2012**, *43*, 3325–3337. [CrossRef]
3. Assler, H. Design of Aircraft Structures under Special Consideration of NDT. 16th World Conference on NDT—2004—Montreal (Canada). 2004. Available online: https://www.ndt.net/?id=2093 (accessed on 27 April 2023).
4. Fortes, L. FSW Applied on Mid Size Aircraft. In Proceedings of the Conference: Aeromat 20 Conference and Exposition American Society for Metals, Cumberland, RI, USA, 9–11 June 2009.
5. Friction Stir Welding of Airframe Structures. Available online: https://www.twi-global.com/who-we-are/who-we-work-with/industry-sectors/aerospace/joining-of-airframe-structures/friction-stir-welding-of-airframe-structures (accessed on 20 April 2023).
6. EMBRAER Official Website. Available online: https://embraer.com/global/en (accessed on 20 April 2023).
7. Han, B.; Tao, W.; Chen, Y.; Li, H. Double-sided laser beam welded T-joints for aluminum-lithium alloy aircraft fuselage panels: Effects of filler elements on microstructure and mechanical properties. *Opt. Laser Technol.* **2017**, *93*, 99–108. [CrossRef]
8. Lin, Y.; Zheng, Z. Microstructural evolution of 2099 AlLi alloy during friction stir welding process. *Mat. Charact.* **2017**, *123*, 307–314. [CrossRef]
9. Momeni, M.; Guillot, M. Effect of Tool Design and Process Parameters on Lap Joints Made by Right Angle Friction Stir Welding (RAFSW). *J. Manuf. Mater. Process.* **2019**, *3*, 66. [CrossRef]
10. Khalafe, W.H.; Sheng, E.L.; Bin Isa, M.R.; Omran, A.B.; Shamsudin, S.B. The Effect of Friction Stir Welding Parameters on the Weldability of Aluminum Alloys with Similar and Dissimilar. *Met. Rev. Met.* **2022**, *12*, 2099. [CrossRef]
11. Aldanondo, E.; Vivas, J.; Álvarez, P.; Hurtado, I. Effect of Tool Geometry and Welding Parameters on Friction Stir Welded Lap Joint Formation with AA2099-T83 and AA2060-T8E30 Aluminium Alloys. *Metals* **2020**, *10*, 872. [CrossRef]
12. Aldanondo, E.; Vivas, J.; Álvarez, P.; Hurtado, I.; Karanika, A. Friction Stir Welding of AA2099-T83 and AA2060-T8E30 Aluminium Alloys with New Cr-Free Surface Treatments and Sealant Application. *Metals* **2021**, *11*, 644. [CrossRef]
13. Aldanondo, E.; Zubiri, O.; Vivas, J.; Álvarez, P.; Hurtado, I. Fretting Fatigue as a Limiting Factor on the Durability of Friction Stir Welded Lap Joints Using AA2099-T83 and AA2060-T8E30 Aluminium Alloys. *J. Manuf. Mat. Proc.* **2022**, *6*, 94. [CrossRef]
14. Reuter, M.A.; Hudson, C.; Van Schaik, A.; Heiskanen, K.; Meskers, C.; Hagelüken, C. *Metal Recycling: Opportunities, Limits, Infrastructure*; A Report of the Working Group on the Global Metal Flows to the International Resource Panel; UNEP, Ed.; International Resource Panel, Working Group on the Global Metal Flows: Nairobi, Kenya, 2013; ISBN 978-92-807-3267-2.
15. The Aluminum Association. *Aluminum Industry Technology Roadmap*; The Aluminum Association: Washington, DC, USA, 2003.
16. Bureau of International Recycling (BIR). Available online: https://www.bir.org (accessed on 21 December 2020).
17. Krause, G. Markets for Steel and Aluminium Scrap, GMTN 2019—Specialist Article No. 5 November 2018, Mediakonzept, Düsseldorf. Available online: https://www.newcast.com/en/Media_News/Press_material/Professional_articles/Markets_for_Steel_and_Aluminium_Scrap (accessed on 27 April 2023).
18. Gaustad, G.; Olivetti, E.; Kirchain, R. Improving aluminium recycling: A survey of sorting and impurity removal technologies. *Resour. Conserv. Recycl.* **2012**, *58*, 70–87. [CrossRef]
19. Raabe, D.; Ponge, D.; Uggowitzer, P.J.; Roscher, M.; Paolantonio, M.; Liu, C.; Antrekowitsch, H.; Kozeschnik, E.; Seidmann, D.; Gault, B.; et al. Making sustainable aluminum by recycling scrap: The science of "dirty" alloys. *Progr. Mat. Sci.* **2022**, *128*, 100947. [CrossRef]
20. Meng, L.; Zheng, X.L. Overview of the effects of impurities and rare earth elements in Al-Li alloys. *Mater Sci. Eng. A* **1997**, *237*, 109–118. [CrossRef]
21. Efthymiou, E.; Cöcen, Ö.N.; Ermolli, S.R. Sustainable aluminium systems. *Sustainability* **2010**, *2*, 3100–3109. [CrossRef]
22. Sentry Project Reporting. Available online: https://cordis.europa.eu/project/id/632487/reporting (accessed on 27 April 2023).
23. Arnaiz, S.; Arieta-araunabeña, M.; Fernández-Calvo, A.I.; San Sebastian, M. Environmental assessment of the EoL phase of the B2 Demonstrators—Low weight green metallic fuselage panels including dismantling and recycling. In Proceedings of the EARS 2016: The Third European Aircraft Recyling Symposium, Stuttgart, Germany, 16–17 March 2016.
24. EcoTech Project. Available online: https://www.clean-aviation.eu/sites/default/files/2021-10/CLEAN_SKY_Article_EcoTech.pdf (accessed on 27 April 2023).
25. A Safer, Non-Toxic Alternative for Paint Stripping. Available online: https://adapt-laser.com/paint-stripper-alternative/ (accessed on 27 April 2023).
26. Luey, K.; Coleman, D.; Ternet, G. Replacement of Methylene Chloride in NVR and Paint Removal Applications, DTIC Document. 2000. Available online: https://apps.dtic.mil/sti/pdfs/ADA388362.pdf (accessed on 27 April 2023).
27. European Chemicals Agency. Annex XVII to Reach—Conditions of Restriction Restrictions on the Manufacture, Placing on the Market and Use of Certain Dangerous Substances, Mixtures and Articles. Available online: https://echa.europa.eu/documents/10162/0ea58491-bb76-4a47-b1d2-36faa1e0f290 (accessed on 27 April 2023).
28. Nyarko, E. *Determination of the Relative Activity of Selected Paint Stripping Components with Epoxy and Polyurethane Aerospace Coatings*; OhioLINK ETD, Nyarko, Ebenezer: Kumasi, Ghana, 2011.

29. Aldanondo, E.; Arruti, E.; Iturrioz, A.; Huarte, I.; Zubiri, F.; Hurtado, I. Welding Technology Developments for Stringer-Skin Joints with Al-Li Alloys. *J. Light Met. Weld.* **2020**, *58*, 65s–71s. [CrossRef]
30. The Aluminum Association. TEAL Sheets. 2015. Available online: https://www.aluminum.org/sites/default/files/2021-11/TealSheet.pdf (accessed on 18 December 2018).

Disclaimer/Publisher's Note: The statements, opinions and data contained in all publications are solely those of the individual author(s) and contributor(s) and not of MDPI and/or the editor(s). MDPI and/or the editor(s) disclaim responsibility for any injury to people or property resulting from any ideas, methods, instructions or products referred to in the content.